Dalton Transactions

Accepted Manuscript

ROYAL SOCIETY OF CHEMISTRY

www.rsc.org/dalton

Journal Name

RSCPublishing

ARTICLE

Charge-bistable Pd(III)/Pd(II,IV) coordination polymers: phase transitions and their applications to optical properties

Shohei Kumagai,[a,b] Shinya Takaishi,*[a,c] Hiroaki Iguchi[a,c] and Masahiro Yamashita*[a,b,c]

Cite this: DOI: 10.1039/x0xx00000x

Received 00th January 2012,
Accepted 00th January 2012

DOI: 10.1039/x0xx00000x

www.rsc.org/

Quasi-one-dimensional halogen-bridged Pt, Pd, and Ni complexes (MX chains) are a family of materials with potential charge bistability: M(II)–M(IV) mixed valence charge-density-wave (CDW) and M(III) averaged valence Mott–Hubbard (MH) states can form. However, until recently, no examples of MX chains showing charge bistability were reported. Charge-bistable Pd MX chains, $[Pd(en)_2Br](\mathbf{Y1\text{-}C}_n)_2\cdot H_2O$ (en = 1,2-diaminoethane; $\mathbf{Y1\text{-}C}_n$ = dialkyl 2-sulfosuccinate; n = the number of carbon atoms in alkyl chains) and $[Pd(en)_2Br](\mathbf{Y2\text{-}C}_n)_2\cdot H_2O$ ($\mathbf{Y2\text{-}C}_n$ = dialkyl α-sulfomalonate), both of which showed phase transitions between Pd(III) MH and Pd(II,IV) CDW states, were prepared by utilizing chemical pressure. In addition, $[Pd(en)_2Br](\mathbf{Y1\text{-}C}_n)_2\cdot H_2O$ underwent pressure- and photo-induced MH-CDW phase transitions. $[Pd(en)_2Br](\mathbf{Y2\text{-}C}_n)_2\cdot H_2O$ has a higher transition temperature, i.e., higher stability of the MH state, than $[Pd(en)_2Br](\mathbf{Y1\text{-}C}_n)_2\cdot H_2O$ does due to the difference in the crystal packing. The recent progress will lead to new pressure sensing and optical switching devices.

1 Introduction

Bistable molecular solids, in which electronic states can be switched by external stimuli, such as temperature (T), magnetic field, electric field, pressure (P) and light, have potential applications in memory storage devices, sensors, etc.[1] Recently, it has been thought that condensed molecular solids, such as coordination polymers, with the cooperative bistabilities should exhibit gigantic responses to stimuli, although such materials are rare.

Quasi-one-dimensional halogen-bridged transition metal (Pt, Pd and Ni) complexes are condensed molecular solids with one-dimensional (1D) linear chain structures composed of metal (M) ions and bridging halide (X) ions. On the basis of the number of M ions per unit, these complexes are classified into two systems: mononuclear (MX chains) and dinuclear complexes (MMX chains). MMX chains form the chain structures consisting of paddle-wheel dinuclear metal units and X ions, such as $[M_2(S_2CR)_4X]$ (M = Ni and Pt; R = alkyl-chain group)[2] and $[Pt_2(P_2H_2O_5)_4X]^{4-}$,[3] i.e., ···M–M–X–M–M–X···. It has been theoretically[4] and experimentally shown that MMX chains can form four electronic states, and a variety of physical properties, such as a high electrical conductivity, metal–insulator transition and negative differential resistance, have been reported so far.[3,5]

In MX chains, M ions and X ions alternate along the chain, which is represented as ···M–X–M–X···. Moreover, the chain is connected together via the d_{z^2} orbitals of M ions and the p_z orbitals of X ions (Figure 1a). MX chains are classified as extended Peierls–Hubbard system,[6] where the electron–lattice interaction (S), the transfer integral (t), and the on-site and nearest-neighbour Coulomb repulsions (U and V, respectively) strongly compete and cooperate with each other. According to the simplest understanding, the competition between S and U determines the ground electronic state. An M(II)–M(IV) mixed valence charge-density-wave (CDW) state is formed when $S > U$ (Figure 1c), whereas an M(III) averaged valence Mott–Hubbard (MH) state is formed when $U > S$ (Figure 1b). The chain

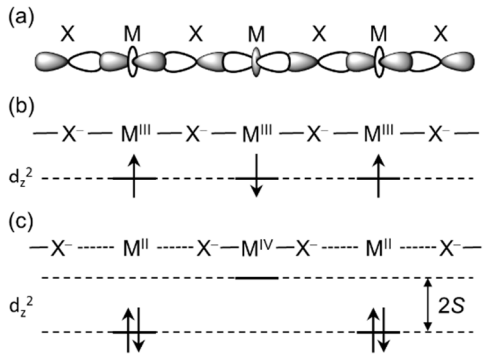

Figure 1. Schematic illustrations of (a) the 1D chain for MX chains and the electronic structure of the (b) MH and (c) CDW states.

structures of MX chains for MH and CDW states are expressed as ···M^{III}–X–M^{III}–X··· and ···M^{IV}–X—M^{II}—X···, respectively. Thus, MX chains have potential charge bistability. In an MH state, X ions are located at the midpoints between neighbouring M^{III} ions, and the antiferromagnetic interactions act between the electron spins (total spin quantum number = 1/2) in the M d_z^2 orbitals along the chain. An MX chain in an MH state is classified as a Robin–Day class III mixed valence complex.[7] On the other hand, the M ions disproportionate, and the X ions become displaced towards the M^{IV} ions in a CDW state. This state is classified as Robin–Day class II.[7]

The first reported MX chain was the so-called Wolfram's red salt $[Pt^{II}(NH_2C_2H_5)_4][Pt^{IV}Cl_2(NH_2C_2H_5)_4]Cl_4{\cdot}4H_2O$, which is in a CDW state.[8] Since its discovery in 1900, MX chains have been intensively investigated because of their solid-state properties, such as intense and dichroic charge-transfer (CT) bands,[9] overtone progressions in the resonant Raman spectra,[10] and midgap absorptions attributed to solitons and polarons,[11] due to the 1D system and the mixed valence states. It has been shown that most Pt and Pd MX complexes are in CDW states.

The first MH complex with M = Ni was reported in 1989.[12] In contrast with the Pd and Pt MX chains, all of the Ni MX chains so far reported are in Ni(III) MH states. In addition, they have been reported to exhibit various characteristic properties, such as gigantic third-order nonlinear optical susceptibilities,[13] ultrafast optical switching from MH state to metal[14] and spin-Peierls transitions.[15] In particular, their optical characteristics are expected to be promising for application in all-optical ultrafast switching devices.[16]

Although MX chains have potential for charge bistability, Ni MX chains have been reported to form only MH states, and Pd and Pt MX chains form CDW states. This is caused by the different U values for the M ions: 6.0, 1.5, and 1.0 eV for Ni,[17] Pd,[18] and Pt ions,[6] respectively. Thus, the ability of MX chains to exhibit charge bistability has been called into question. On the basis of extended Peierls–Hubbard theory, a CDW–MH phase transition will occur when S and U are comparable to each other ($S \approx U$).

Moreover, from the viewpoint of the potential energy curve of the X ion, the bistability of the electronic states can be explained as follows. If the M–X bond is ionic, the potential energy of the X ion is expressed by the Born–Mayer equation. In a mixed valence system, the X ions are in a double-minimum potential energy, which is composed of the sum of potential energy curves for the M^{IV}–X—M^{II} and M^{II}—X–M^{IV} local structures,[19] as shown in Figure 2. Here the potential energy minimums approach each other with a decrease in the neighboring M–M distance, which is similar to a decrease in S. Eventually, the potential energy forms a single-minimum potential, indicating a transition from a CDW to an MH state. Since the M–M distance can be shortened by applying pressure, several high-pressure studies have been performed on complexes with short M–M distances, such as $[Pd(chxn)_2][Pd(chxn)_2Br_2]Br_2$ (chxn = 1*R*,2*R*-diaminocyclohexane).[20] However, no evidence of a CDW–MH transition has been reported yet.

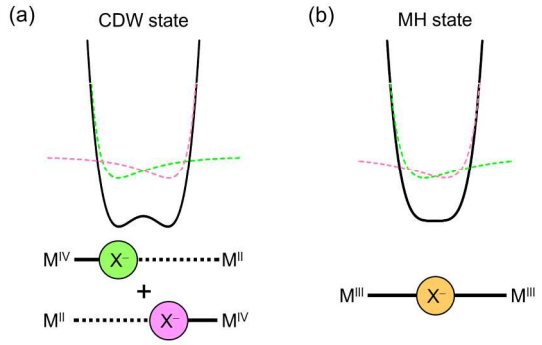

Figure 2. Schematic illustration of potential energy curves of the X ions in (a) a CDW state and (b) an MH state. Dotted lines depict the potential energy curves attributable to an M–X–M local structure. Black solid line expresses the sum of the curves between the neighbour sites.

Yamashita and co-workers have reported a bromide-bridged Pd compound with the Pd(III) MH state by using attractive chemical pressure acting between alkyl chains. In 2008, a series of dialkyl 2-sulfosuccinato ions (**Y1-C$_n$**; n: the number of carbon in alkyl chains; see Scheme 1) was used as counterions, and the bromide-bridged Pd compounds underwent the phase transitions between CDW states in the high-T phase and MH states in the low-T phase.[21] The transition T (T_c) values depended on n. This was the first example of an MX chain exhibiting a CDW–MH phase transition. In addition, they later reported an analogous Pd complex with dialkyl α-sulfomalonate counterion (**Y2-C$_n$**; see Scheme 1),[22] which had a higher T_c than that of the **Y1-C$_n$** complex. The complexes with **Y1-C$_n$** were further investigated to determine if they underwent pressure-induced[23] and photo-induced[24] phase transitions. The latter phenomenon could be used in the development of optical switching and memory storage.[16] Herein we review the recent progress in the preparation of charge bistable Pd(III)/Pd(II,IV) MX chains. In the next chapter, we describe how a charge bistability, i.e., a CDW–MH phase transition, has been realized and confirmed from the viewpoint of temperature dependency. Following that, the further findings, a pressure- and a photo-induced phase transitions, which supply practical demonstrations of the charge bistability, are

demonstrated. Note that Table 1 summarizes brief information on the compounds discussed in this paper.

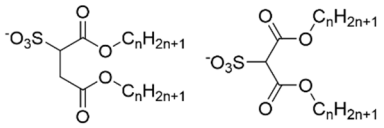

Scheme 1. Chemical structures of the counterions **Y1-C$_n$** and **Y2-C$_n$**. Adapted from Ref. 22.

Table 1. Selected information on the compounds

Compound	**1-C4**[†]	**1-C5**	**1-C5**	**2-C7**
T / K	295	162(2)	259(2)	293(2)
Crystal system	—	Monoclinic	Monoclinic	Triclinic
Space group	—	$P2$	$C2$	$P1$
d / Å	5.346	5.217	5.280	5.207
Electronic state	CDW	MH	CDW	MH
T_c / K	—		206	310
P_c / GPa	1.2		—	—
Ref.	23		21	22

[†]Single-crystal structure is not reported. The d is obtained from a plot in Ref. 23.

2. Temperature-induced phase transition in the Pd MX chains [Pd(en)$_2$Br](Y1-C$_n$)$_2$·H$_2$O and [Pd(en)$_2$Br](Y2-C$_n$)$_2$·H$_2$O by using attractive chemical pressure

2.1 Synthetic strategy

As the counterions are bulky, a small diamine molecule, 1,2-diaminoethane (en), is used as the in-plane ligand (L). The desired Pd complexes crystallize during the oxidation of $[Pd(en)_2]^{2+}$ by slow diffusion of Br_2 into the appropriate solvent in the presence of a sodium salt of the counterion. Because of the solubility, a mixture of water and polar organic solvent, such as methanol and tetrahydrofuran, are used. In addition, an electrochemical oxidation method with tetrabutylammonium bromide as an electrolyte can be also utilized. In this paper, the obtained Pd MX chains, [Pd(en)$_2$Br](**Y1-C$_n$**)$_2$·H$_2$O and [Pd(en)$_2$Br](**Y2-C$_n$**)$_2$·H$_2$O, are abbreviated as **1-C*n*** and **2-C*n***, respectively.

2.2 Crystal structure

A crystal structure of **1-C5** at 162 K is shown in Figure 3a.[21] The complex has a linear chain structure composed of Pd ions and Br ions, which is surrounded by **Y1-C$_5$** counterions and crystallization waters (omitted in this figure). In the crystal packing, there is a clear lamellar structure consisting of hydrophilic 1D chain layers and hydrophobic alkyl-chain layers stacked along the c axis (Figure 3b). At 259 K, the structure (not shown) was similar to that at 162 K. However, several differences, such as space group and cell parameters, were observed. The space group changed from $P2$ at low T to $C2$ at high T. In addition, the lattice parameters a and b at 259 K were determined to be two times longer than those at 162 K. At 259 K, the Pd(1)–Br bond lengths were 2.512 and 2.497 Å, whereas the Pd(2)–Br bond lengths were 2.783 and 2.776 Å (Figure 3d left). Since Pd^{IV}–Br bond lengths are shorter than Pd^{II}–Br ones are, Pd(1) and Pd(2) were assigned to be Pd^{IV} and Pd^{II}, respectively. At 162 K, the Pd ions became equivalent, and the Pd–Br bond lengths were 2.613 and 2.604 Å. These structural features indicated that **1-C5** underwent a CDW-MH phase transition.

The T dependence of the nearest-neighbor Pd–Pd distances (d) in **1-C5** was studied to discuss the phase boundary. In Figure 4,

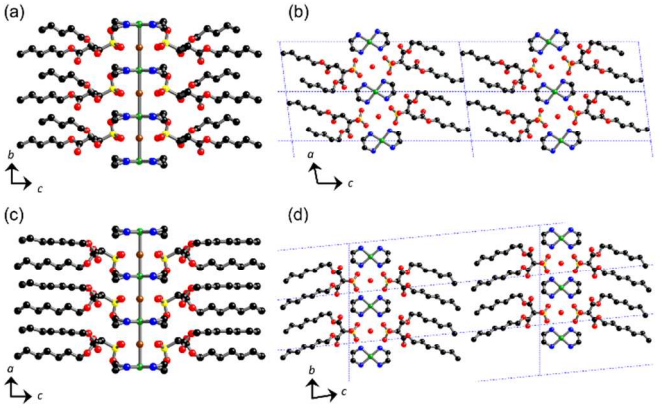

Figure 3. Crystal structures of 1-C5 at 162 K along (a) a and (b) b axes and of 2-C7 at 293 K viewed along (c) b and (d) a axes. C, black; N, blue; O, red; S, yellow; Br, brown; Pd, green. Hydrogen atoms are omitted for clarity. Crystallization waters are omitted in (a) and (c) for clarity. Blue broken lines indicate the unit cells.

d is plotted as a function of T. d of **1-C5** at 293 K was 5.31 Å, which decreased by *ca.* 2% with a decrease in T to 110 K to become 5.21 Å. This was the first observation of such a large T dependence of d for other MX chains. In this case, the thermal motion of the alkyl chains in the counterions was suppressed, as shown by the small T factors of the carbon atoms in the alkyl chains at 162 K compared with those at 259 K. Furthermore, hysteresis in d was observed at *ca.* 205 K. This indicated that a first-order phase transition occurred at this T. In addition, a d value of 5.26 Å appears to be the boundary between the MH and CDW states.

In Figure 3c, the crystal structure of **2-C7**, in which the counterion used has been modified to change the crystal packing and to control T_c,[22] at 293 K is shown. **2-C7** crystallized in the space group $P1$. Viewed from the b axis, however, **2-C7** is structurally similar to **1-C5** and has a lamellar packing structure (Figure 3d). Unlike **1-C5**, all of the Pd ions were equivalent at this T. The Pd–Br bond lengths were 2.600 and 2.606 Å, and d was 5.206 Å, which was shorter than the boundary length (5.26 Å). These features indicated that the electronic state of **2-C7** at room T was an MH state. Furthermore, this was the first crystal structure of a Pd MX chain in an MH state at room T.

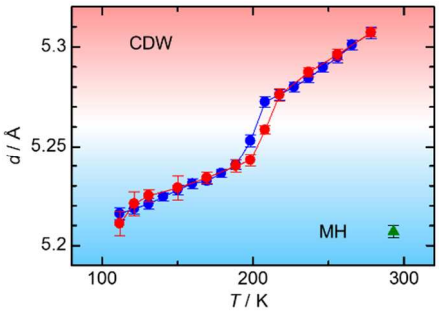

Figure 4. *T* dependence of *d*. Circle, **1-C5** (red and blue for heating and cooling, respectively); triangle, **2-C7**. Pink and blue shadows indicate the regions of CDW and MH states, respectively.

2.3 X-ray diffraction analysis

In addition to the crystal structure determination, various physical measurements were performed to investigate the phase boundary in both **1-C5** and **2-C7**. X-ray diffraction (XRD) patterns of both complexes at various *T* were compared. In Figure 5, X-ray oscillation photographs at several *T* are shown. For MX chains, these photographs are often used to estimate the electronic state because diffuse scatterings or superlattice reflections, which originate from 2-fold periodicity along the 1D chain direction, can be observed in the CDW states. For **1-C5** (Figures 5a–5c), superlattice reflections were clearly observed above 206 K, but they disappeared below 204 K. The boundary T_c was consistent with that estimated from the *d*–*T* plot in Figure 4. For **2-C7**, no diffuse scatterings were observed up to 303 K. Weak diffuse scatterings, however, appeared above 308 K, indicating that the T_c for **2-C7** was *ca.* 308 K.

The single crystal structure of **2-C7** in the CDW state could not be determined, although that of **1-C5** was determined. For **1-C5**, clear superlattice reflections and the single crystal structure indicated that it was in a 3D-ordered CDW state. On the other hand, the XRD pattern of **2-C7** at high *T* showed only weak diffuse scatterings, supporting that it is in a CDW state with low dimensional ordering.

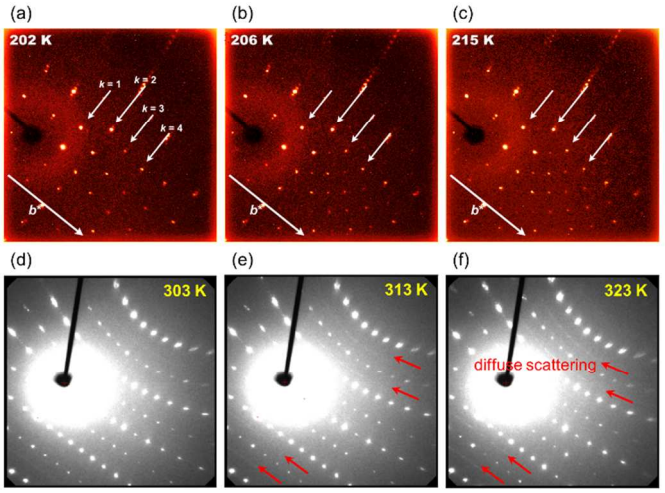

Figure 5. X-ray oscillation photographs for **1-C5** at (a) 202, (b) 206, and (c) 215 K, and for **2-C7** at (d) 303, (e) 313, and (f) 323 K. The white arrows in (a)–(c) indicate the directions of *b** and planes with *k* = 1–4. The red arrows in (d)–(f) point to the diffuse scatterings. (d)–(f) adopted from Ref. 22.

2.4 Optical conductivity spectroscopy

In Figure 6, the optical gaps (E_{CT}) of **1-C5** and **2-C7** are plotted as a function of *T*. E_{CT} was determined from the peak tops in optical conductivity spectra, which were obtained by Kramers–Krönig transformation[25] of the polarized reflectivity spectra with the polarization parallel to the chain directions. The measurements were performed below room *T*. The E_{CT} for **1-C5** was determined to be 0.86 eV at 290 K and decreased to 0.66 eV at 210 K. A discontinuous change was clearly observed at 206 ± 2 K. Below this *T*, E_{CT} was *ca.* 0.58 eV independent of *T*. On the other hand, for **2-C7**, E_{CT} was determined to be *ca.* 0.58 eV, and it remained constant below 293 K.

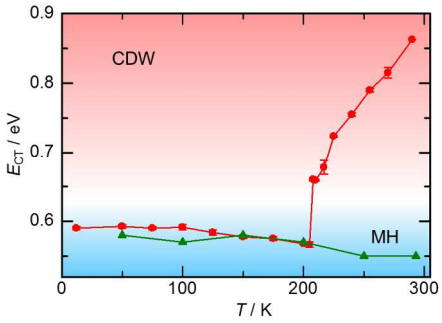

Figure 6. *T* dependence of E_{CT} for **1-C5** (circle) and **2-C7** (triangle). Pink and blue shadows indicate the regions of CDW and MH states, respectively.

Schematic illustrations of the band structure of the MX chains are shown in Figure 7. According to the extended Peierls–Hubbard model,[6] for an MH state, E_{CT} is expressed as $E_{CT} \approx U$ if *V* is ignored (Figure 7a). This transition is attributed to that from the lower-Hubbard band (LHB) to the upper-Hubbard band (UHB), which are produced due to splitting of the half-filled Pd $4d_z^2$ band via strong Coulomb repulsion. Because *U* is the same for identical complexes, E_{CT} does not change in the MH state when *T* changes. On the other hand, for a CDW state,

E_{CT} is expressed as $E_{CT} \approx 2S - U$ if V is ignored (Figure 7b). This transition is attributed to that from Pd^{II} $4d_z^2$ to Pd^{IV} $4d_z^2$. In this expression, S depends on d, whereas U is constant. Thus, for the present Pd MX chains in the CDW state, E_{CT} can be tuned by changing d (or T). In other words, the electronic ground states of **1-C*n*** and **2-C*n*** are MH and CDW states in low-T and high-T phases, respectively, which is in agreement with the structural study.

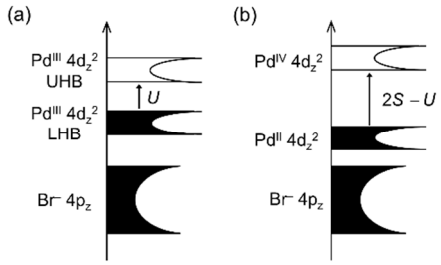

Figure 7. Schematic illustrations of the band structures of bromide-bridged Pd MX chains in (a) MH and (b) CDW states. Arrows express the lowest electronic transition attributed to E_{CT}.

2.5 Fabrication of thin films and their optical properties

For practical applications, it must be possible to prepare thin films of the MX chains. However, this has been difficult because vacuum deposition and dispersion techniques from organic solvents cannot be used. Using a transparent polymer, poly(methyl methacrylate) (PMMA), as matrix, a thin film of a Ni MX chain $[Ni^{III}(hxdn)_2Br]Br_2$ (hxdn = 1,2-diaminohexadecane) has been prepared on a CaF_2 substrate.[26] The Ni MX chain-PMMA composite exhibited ultrafast optical switching ability. The key strategy for preparing the composite was to use long alkyl chains in L, i.e., hxdn, which improved the solubility of the MX chains in organic media. Since a dispersion of $[Pt(en)_2][PtCl_2(en)_2]$(**Y1-C$_{12}$**)$_4$ in chloroform had been already reported,[27] it was expected that Pd complexes with similar counterions could be dispersed and that films of these complexes could be fabricated the same way that $[Ni^{III}(hxdn)_2Br]Br_2$ was. In Figure 8, an absorption spectrum of a thin film of **2-C12**, which is analogous to **2-C7** but with a bulkier counterion, fabricated on an SiO_2 substrate (red line) is shown. The dispersions of the MX chains were remarkably stable when n was larger. In other words, **2-C12** was more suitable than **2-C7** was for fabricating thin films. The spectrum of the thin film of **2-C12** was consistent with that of a single crystal of **2-C7**, indicating that, like **2-C7**, the ground state of the thin film of **2-C12** was an MH state at room T, and that these Pd(III) MX chains can be utilized for optical switching.

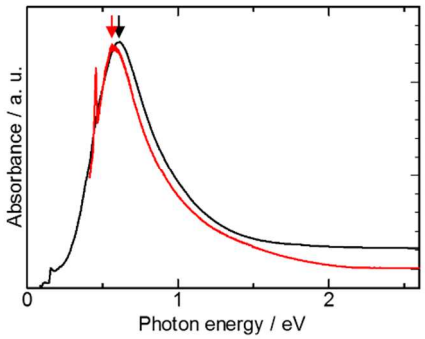

Figure 8. Electronic spectra of **2-C7** single crystal (black line) and **2-C12** thin film of SiO_2 substrate (red line) at room T. The arrows indicate the CT transition peaks.

2.6 Infrared (IR) spectroscopy

Okaniwa *et al.* reported that it was possible to estimate the electronic states by using IR spectroscopy.[28] When alkylamine was used as L, the N–H vibrational energy varied depending on the valence of the M ion to which the amine nitrogen coordinated. Thus, a complex in an MH state, such as $[Ni^{III}(chxn)_2Br]Br_2$, shows an N–H stretching (ν(N–H)) band at *ca*. 3010 cm^{-1}, whereas a compound in a CDW state, such as $[Pt^{II}(chxn)_2][Pt^{IV}(chxn)_2Br_2]Br_2$, shows two bands at 2995 and 3050 cm^{-1} at room T.[28] We acquired polarized IR spectra for **1-C5** and **2-C7** with the light polarization perpendicular to the chains to ignore the contribution of the CT transition along the chain and the asymmetric ν(N–H). As shown in Figure 9a, two IR bands were observed for **1-C5** at 300 K. This was because of the mixed valence nature, i.e., $Pd^{II,IV}$. With a decrease in T, the peak positions of these bands slightly approached each other, and below 210 K, they coalesced, suggesting that a phase transition to an MH state occurred. On the other hand, **2-C7** showed a single ν(N–H) band at 290 K, and this band split at 310 K (Figure 9b). In other words, a phase transition from an MH state to a CDW state occurred. The spectral changes are plotted as the ν(N–H) peak position is plotted as a function of T in Figure 9c.

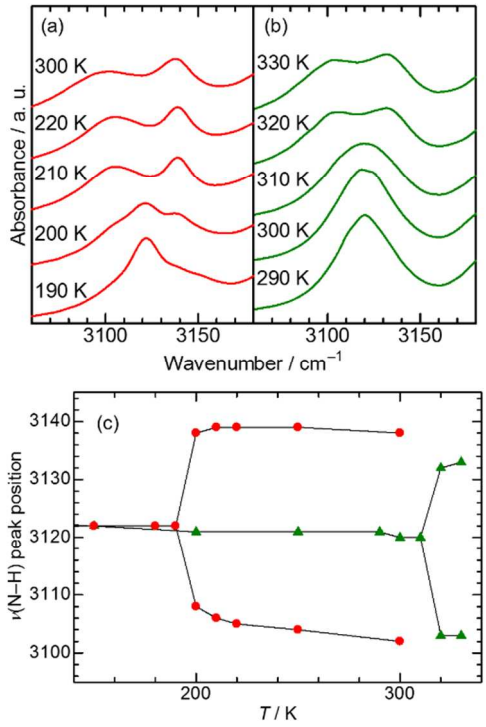

Figure 9. Variable-*T* (VT) IR spectra of (a) **1-C5** and (b) **2-C7**. (c) ν(N–H) vs. *T*. Circle, **1-C5**; triangle, **2-C7**.

2.7 Electron spin resonance (ESR) spectroscopy

Since the magnetic ground states of MH and CDW states are different, the spin susceptibility should be affected when a CDW–MH phase transition occurs. However, because the difference in the magnetic susceptibilities of the MH and CDW states was small (~10^{-5}–10^{-6} emu mol^{-1}), which was much smaller than diamagnetic susceptibility arising from ligands, counterions, and inner shell of M ions, a superconducting quantum interference device could not be used. Therefore, ESR spectroscopy was performed at various *T*. The spin susceptibility (χ) were then obtained by integrating the first derivative of the ESR signal twice, using $CuSO_4 \cdot 6H_2O$ as an external standard. The *T* dependence of χ for **1-C5** and **2-C7** are shown in Figures 10a and 10b, respectively. The CDW–MH phase transition was observed as an increase in χ near 210 K and 310 K for **1-C5** and **2-C7**, respectively. Not only the CDW state but also the MH state are in principle diamagnetic since strong antiferromagnetic interactions are present among the nearest-neighbour M ions along the chains in the MH state. The origin of the ESR signal arises from defect Pd(III) sites in both states and from the terminal Pd(III) ions in the chains composed of odd-numbers of Pd ions in an MH state. In other words, in the same sample, larger number of electron spins exist in an MH state than in a CDW state, as shown in the χ vs. *T* plot in Figure 10. The χ for the low-*T* phase was higher than that for the high-*T* phase, and T_c was consistent with the studies discussed above. The jumps in the χ values indicate that a CDW–MH phase transition occurs. The χ value was slightly smaller for **2-C7** than it was for **1-C5** over the entire *T* range. In addition, no hysteresis was observed in the case of **2-C7**, whereas there was clear hysteresis in the case of **1-C5** near T_c. There was a gradual decrease in χ for **2-C7** below 200 K. This behavior was similar to that for $[Ni^{III}(chxn)_2Br]Br_2$, which was confirmed to undergo a spin-Peierls transition.[15a] Although further investigation is needed, **2-C7** is a candidate for use as a spin-Peierls material.

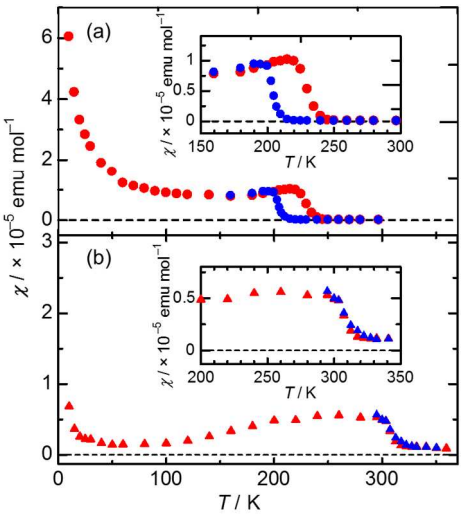

Figure 10. *T* dependence of χ for (a) **1-C5** and (b) **2-C7**. Red and blue symbols indicate the heating and cooling processes, respectively. Insets are the magnification of the corresponding plots for each compound with the appropriate *T* ranges.

2.8 Electrical conductivity

Direct-current electrical resistivity measurements were performed on **1-C5** and **2-C7**. In Figure 11, the electrical resistivity (ρ) along the chains upon heating are plotted as a function of T^{-1} (lower axis) and as a function of *T* (upper axis). As shown in Figure 7, the electronic structures predict that both the MH and CDW states will exhibit semiconductor-type conduction behaviors. For both complexes, in the low-*T* region, ρ decreased with an increase in *T*, which indicated semiconductor-type conduction behaviour. The activation energies were calculated to be 103 and 68 meV for **1-C5** and **2-C7**, respectively. As these values were much smaller than that expected from E_{CT}, it was concluded that an indirect transition occurred in these complexes. Furthermore, ρ became a minimum near 210 and 310 K for **1-C5** and **2-C7**, respectively. These *T* values are consistent with the T_c estimated from the experimental results discussed above, indicating the occurrence of a CDW–MH phase transition. Followed by a steep increase, ρ gradually increased with an increase in *T* in the high-*T* region, which is metallic-like *T* dependency. However, a CDW state should show semiconductor-type *T* dependency. This inconsistency was explained by the *T* dependence of E_{CT} accompanied by drastic shrinking of the 1D chains at low *T*.

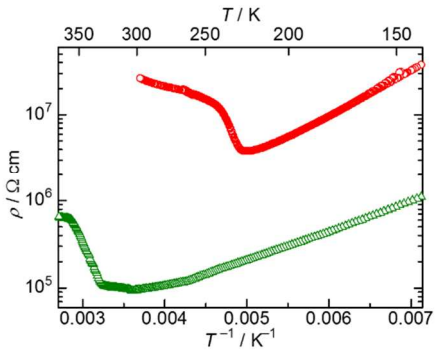

Figure 11. Electrical resistivity ρ along the chain for **1-C5** (red circle) and **2-C7** (green triangle).

2.9 Comparison of the T_c values for 1-C*n* and 2-C*n*

In Figure 12, the T_c values for **1-C*n*** and **2-C*n*** were plotted as a function of n. The T_c of **1-C*n*** with $n \geq 6$ were determined from VT Raman spectra.[21,23] For **1-C*n***, the T_c values increased with an increase in n. The T_c value for **2-C7** (*ca.* 310 K) was greater by 45 K than that for **1-C7** (*ca.* 265 K). As M, X, L and n used for syntheses of **1-C*n*** and **2-C*n*** were the same, the differences in the packing structures and the differences in the structures of the counterions caused the remarkable increase in T_c. However, further studies are needed to determine the most important factor for stabilizing the MH state.

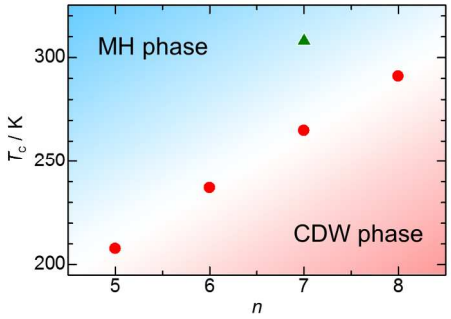

Figure 12. n dependence of T_c for **1-C*n*** (circle) and **2-C*n*** (triangle). Pink and blue shadows express the areas assignable to MH and CDW states, respectively, in **1-C*n***.

3 Pressure-induced phase transition in 1-C4

Although **1-C5** underwent a CDW–MH phase transition, no MH state for **1-C4** was observed even at 10 K,[23] implying that the attractive chemical pressure was not enough to induce a phase transition even at low T. Thus, Matsuzaki *et al.* tried to induce a CDW–MH phase transition with hydrostatic pressure while observing the changes in the Raman spectra.[23]

They acquired VT Raman spectra for **1-C*n*** with n = 4–9 and 12 at ambient P. At 295 K, strong Raman bands were observed in the range of 110–130 cm^{-1} for **1-C*n*** with n = 4–8. This band was attributed to the symmetric Pd–Br stretching mode ν(Pd–Br). On the other hand, no Raman bands were observed for **1-C*n*** with n = 9 and 12. Since the ν(Pd–Br) mode is Raman active in a CDW state and inactive in an MH state, **1-C*n*** with n = 4–8 were in a CDW state at room T, whereas those with n = 9 and 12 were in an MH state, which was consistent with the results from the structural analyses.[21] In addition, the Raman frequencies ω_S shifted to lower energies with an increase in n and a decrease in T. From a plot of ω_S vs. d for the complexes, it was suggested that ω_S attributed to ν(Pd–Br) could be used to determine d. Thus, the effects of hydrostatic pressure on d can be observed by using Raman spectroscopy.

A high-P study on **1-C4** was performed in a diamond anvil cell at room T. In Figure 13a, ω_S for **1-C4** at room T is plotted as a function of P.[23] ω_S decreased with an increase in the applied P up to 1.20 GPa. The ω_S–P curve looked similar to the ω_S–d curve mentioned above, meaning that d could be measured under pressure in relation to ω_S for the ν(Pd–Br), as shown in Figure 13a. In addition, the Raman band intensity for ν(Pd–Br) mode decreased with an increase in P to 1.26 GPa. The integration intensities of the ν(Pd–Br) band were plotted as a function of P (Figure 13b). The intensities of the band gradually decreased with an increase in P and eventually became zero at P = 1.26 GPa. This result suggested that **1-C4** underwent a CDW–MH phase transition at a critical pressure (P_c) of ~1.2 GPa at room T. This was the first observation of a pressure-induced phase transition amongst MX chains.

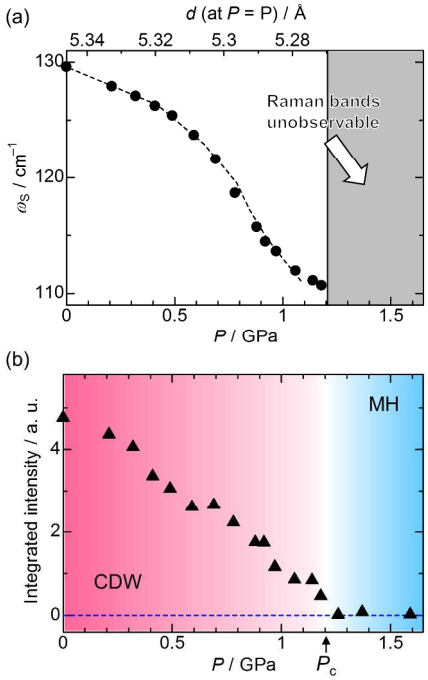

Figure 13. (a) P dependence (lower horizontal axis) of ω_S for **1-C4** at room T. The upper horizontal axis indicates the estimated d at each P. (b) P dependence of the integration intensity of ν(Pd–Br) band at room T. Adopted from Ref. 23. Copyright 2012 Physical Society of Japan.

4 Photo-induced phase transition in 1-C5: selective photo-switching from MH to CDW and to metal states

MX chains have a variety of potential applications. One application is in ultrafast switching of the closely degenerate states in solids by light irradiation, called photo-induced phase transitions, for all-optical switching devices.[16a] In addition, from research on MX chains involving photo-induced phase transitions, some fascinating properties, such as an MH-to-metal transition for an Ni MX chain[14] and a CDW-to-MH transition for a Pd MX chain,[29] have been discovered. However, there are no reports of similar research on Pd(III) MX chains in an MH state because until recently there were no examples of these complexes. The results mentioned above suggest several advantages of using the Pd(III) MH state. Moreover, the closely degenerated MH and CDW states due to charge bistability and the low E_{CT} of ~0.6 eV indicate that its characteristic behaviour is different from that of Ni(III) MX chains in an MH state.

Recently, it was shown that **1-C5** could be selectively converted from the MH to CDW states and from MH to metal states via photo-induced switching.[24] The measurements were performed at 12 K, at which **1-C5** was in an MH state, by using a pump-probe method. The polarized reflectivity was measured with the light electric field parallel to the chain axis, and then spectra of the imaginary part of the dielectric constant (ε_2), which corresponded to the optical conductivity, were obtained by transforming the optical reflectivity spectra using the Kramers–Krönig transformation.[25]

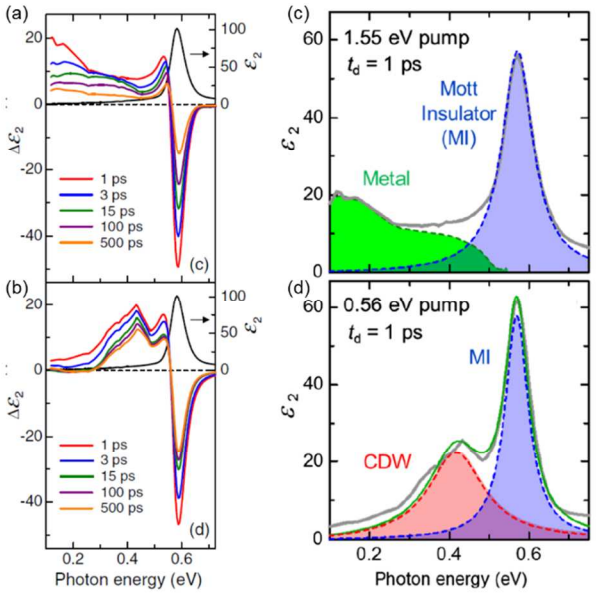

Figure 14. (a,b) Spectrum of ε_2 (black solid line) and its photo-induced changes ($\Delta\varepsilon_2$) at 12 K with t_d of 1, 3, 15, 100, and 500 ps (red, blue, green, purple and orange solid lines, respectively); (a) 1.55 eV pump and (b) 0.56 eV pump. (c,d) ε_2 spectra along the chain of **1-C5** at 12 K and at t_d = 1 ps using (c) 1.55 eV pump and (d) 0.56 eV pump (grey solid lines). Blue shaded areas show the responses of the MH state. Green shaded area in (c) shows the response of the photo-induced metallic state. Red shaded area in (d) shows the response of the photo-induced CDW state. The green solid line in (d) is a fit of the data. Reproduced from Ref. 24. Copyright 2014 American Physical Society.

As shown by the black solid line in Figure 14a, in the ε_2 spectrum of **1-C5** at 12 K, a sharp peak at 0.585 eV was observed, which corresponded to E_{CT} in the MH state.[24] Thus, two photon energies were used to selectively excite **1-C5**: 1.55 eV for high-energy excitation and 0.56 eV for the resonant one. When the complex was irradiated with a 1.55 eV pump, the photo-induced changes in ε_2 ($\Delta\varepsilon_2$) decreased at the original peak energy (0.58 eV) along with an increase in $\Delta\varepsilon_2$ at lower photon energy (Figure 14a), indicating the formation of a metallic state. On the other hand, when a 0.56 eV pump was used, $\Delta\varepsilon_2$ barely changed in the low photon energy region, whereas the original peak intensity changed similar to that when the 1.55 eV pump was used (Figure 14b). Moreover, a peak structure was clearly observed at around 0.4 eV.

The observed photo-induced states were characterized by analyzing the ε_2 spectra with a time delay (t_d) of 1 ps. As shown in Figure 14c, for the 1.55 eV pump, the ε_2 spectrum could be simulated as a sum of the original CT peak at 0.57 eV and the metallic excitation, as depicted by the blue and green areas, respectively. On the other hand, for the 0.56 eV pump, the ε_2 spectrum could be reproduced as the sum of the original CT peak and a Lorentzian component with a peak at 0.41 eV, as depicted by the blue and red areas, respectively, in Figure 14d. Thus, the 0.41 eV peak generated by the resonant excitation corresponded to a metastable state, and it was thought to be a CDW state. Although the peak energy of 0.41 eV was much smaller than that of the CDW state (> 0.66 eV) for $T > T_c$, this value could be reproduced by applying the extended Peierls–Hubbard model using the d value at 12 K.[24]

Mechanisms for the excitation processes are proposed in Figure 15. Upon high-energy excitation, photogenerated electron and hole carriers act as free carriers because of the nature of the spin-charge separation characteristic of 1D correlated electron systems (Figure 15a).[24] On the other hand, the transition to a CDW state is driven by the creation of a Pd^{II}–Pd^{IV} pair via the resonant excitation (Figure 15b).

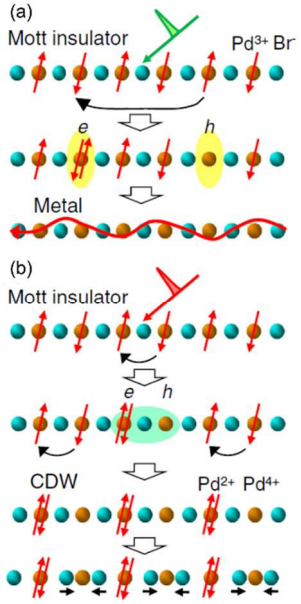

Figure 15. Schematic diagrams of (c) photo-induced MH-to-metal transition and (d) photo-induced MH-to-CDW transition.[24] Reproduced from Ref. 24. Copyright 2014 American Physical Society.

Conclusions

1-C*n* were the first MX chains to show charge bistability. The temperature dependences of the crystal structure, Pd–Pd distance, optical gap, IR spectra, spin susceptibility and electrical conductivity were used to show that **1-C5** underwent a CDW–MH phase transition at 206 K. Attractive chemical pressure acting between alkyl chains reduced the nearest-neighbor Pd–Pd distance, which caused the bistability. After **1-C*n***, **2-C7** was reported to be in an MH state at room *T*. By comparing the T_c values of **1-C7** and **2-C7**, it was found that the crystal packing of **2-C*n*** was suitable for compressing the ···Pd–Br··· 1D chains. Besides the effects of *T*, those of other stimuli have also been studied. A *P*-induced CDW–MH transition at $P_c \approx 1.2$ GPa was observed for **1-C4**, which did not undergo a transition under ambient *P*. This was the first observation of a *P*-induced CDW–MH transition among the MX chains so far reported. Furthermore, **1-C5** was reported to undergo a photo-induced phase transition. The selective photo-induced phase transition is important progress towards practical applications of these complexes. In this case, an MH state was converted to CDW and metallic states by using resonant excitation and high-energy excitation, respectively, at 12 K. The results reviewed here are significant advances towards realizing new devices, such as optical switching, memory storage and pressure-sensing devices.

Finally, it is worth noting that this perspective have described not only the advantages and recent progress of MX chains but also the future prospects of condensed molecular solids for advanced science and technologies. It can be anticipated that there are a lot of undiscovered functional materials, especially condensed molecular solids, which behave like or beyond MX chains shown herein. Hopefully, therefore, this perspective will help many researchers to explore new functional materials, and advanced properties and devices.

Acknowledgements

The authors gratefully acknowledge all collaborators shown in the references for physical measurements and kind discussions. This work was partly supported by a JSPS KAKENHI Grant (A) 26248015 and by a Grant-in-Aid for Young Scientist (B) 25810032.

Notes and references

[a] Department of Chemistry, Graduate School of Science, Tohoku University, 6-3 Aza-Aoba, Aramaki, Aoba-ku, Sendai 980-8578, Japan. E-mail: s-takaishi@m.tohoku.ac.jp, yamasita@agnus.chem.tohoku.ac.jp; Tel (+81)22-795-6544.

[b] WPI-Advanced Institute for Materials Research, Tohoku University, 2-1-1 Katahira, Aoba-ku, Sendai 980-8577, Japan.

[c] CREST, JST, 4-1-8 Honcho, Kawaguchi, Saitama 332-0012, Japan.

1 (a) R. Sessoli, D. Gatteschi, A. Caneschi, M. A. Novak, *Nature*, 1993, **365**, 141; (b) J. A. Real, A. B. Gaspar, M. C. Mũnoz, *Dalton. Trans.*, 2005, 2062; (c) S. Iwai, H. Okamoto, *J. Phys. Soc. Jpn.*, 2006, **75**, 011007; (d) S. Horiuchi, Y. Tokura, *Nat. Mater.*, 2008, **7**, 357; (e) T. Akutagawa, H. Koshinaka, D. Sato, S. Takeda, S. Noro, H. Takahashi, R. Kumai, Y. Tokura, T. Nakamura, *Nat. Mater.*, 2009, **8**, 342; (f) A. Bousseksou, G. Molnár, L. Salmon, W. Nicolazzi, *Chem. Soc. Rev.*, 2011, **40**, 3313; (g) J. S. Miller, *Chem. Soc. Rev.*, 2011, **40**, 3266; (h) W. Zhang, R.-G. Xiong, *Chem. Rev.*, 2012, **112**, 1163; (i) D. N. Woodruff, R. E. P. Winpenny, R. A. Layfield, *Chem. Rev.*, 2013, **113**, 5110; (j) J. Li, Y. Liu, Y. Zhang, H.-L. Cai, R.-G. Xiong, *Phys. Chem. Chem. Phys.*, 2013, **15**, 20786.

2 (a) C. Bellitto, A. Flamini, L. Gastaldi, L. Scaramuzza, *Inorg. Chem.*, 1983, **22**, 444; (b) C. Bellitto, G. Dessy, V. Fares, *Inorg. Chem.*, 1985, **24**, 2815; (c) M. Mitsumi, T. Murase, H. Kishida, T. Yoshinari, Y. Ozawa, K. Toriumi, T. Sonoyama, H. Kitagawa, T. Mitani, *J. Am. Chem. Soc.*, 2001, **123**, 11179; (d) M. Mitsumi, K. Kitamura, A. Morinaga, Y. Ozawa, M. Kobayashi, K. Toriumi, Y. Iso, H. Kitagawa, T. Mitani, *Angew. Chem. Int. Ed.*, 2002, **41**, 2767.

3 (a) C.-M. Che, F. H. Herbstein, W. P. Schaefer, R. E. Marsh, H. B. Gray, *J. Am. Chem. Soc.*, 1983, **105**, 4604; (b) M. Kurmoo, R. J. H. Clark, *Inorg. Chem.*, 1985, **24**, 4420; (c) L. G. Butler, M. H. Zietlow, C.-M. Che, W. P. Schaefer, S. Sridhar, P. J. Grunthaner, B. I. Swanson, R. J. H. Clark, H. B. Gray, *J. Am. Chem. Soc.*, 1988, **110**, 1155; (d) S. Matsunaga, K. Takizawa, D. Kawakami, H. Iguchi, S. Takaishi, T. Kajiwara, H. Miyasaka, M. Yamashita, H. Matsuzaki, H. Okamoto, *Eur. J. Inorg. Chem.*, 2008, 3269; (e) H. Iguchi, S. Takaishi, T. Kajiwara, H. Miyasaka, M. Yamashita, H. Matsuzaki, H. Okamoto, *J. Am. Chem. Soc.*, 2008, **130**, 17668.

4 (a) M. Kuwabara, K. Yonemitsu, *J. Phys. Chem. Solids*, 2001, **62**, 435; (b) M. Kuwabara, K. Yonemitsu, *J. Mater. Chem.*, 2001, **11**, 2163.

5 (a) H. Kitagawa, N. Onodera, T. Sonoyama, M. Yamamoto, T. Fukawa, T. Mitani, M. Seto, Y. Maeda, *J. Am. Chem. Soc.*, 1999, **121**, 10068; (b) K. Otsubo, A. Kobayashi, K. Toriumi, Y. Iso, H. Kitagawa, T. Mitani, *J. Am. Chem. Soc.*, 2006, **128**, 8140; (c) M. Mitsumi, T. Yamashita, Y. Aiga, K. Toriumi, H. Kitagawa, T. Mitani, M. Kurmoo, *Inorg. Chem.*, 2011, **50**, 4368; (d) H. Iguchi, S. Takaishi, D. Jiang, J. Xie, M. Yamashita, A. Uchida, H. Kawaji, *Inorg. Chem.*, 2013, **52**, 13812; (e) H. Iguchi, S. Takaishi, M. Yamashita, *Chem. Lett.*, 2014, **43**, 69; (f) H. Iguchi, A. Nafady, S. Takaishi, M. Yamashita, A. M. Bond, *Inorg. Chem.*, 2014, **53**, 4022.

6 (a) K. Nasu, *J. Phys. Soc. Jpn.*, 1984, **52**, 3865; S. M. Webber-Milbrodt, J. T. Gammel, A. R. Jr. Bishop, *Phys. Rev. B*, 1992, **45**, 6435; (b) K. Iwano, K. Nasu, *J. Phys. Soc. Jpn.*, 1992, **61**, 1380.

7 M. B. Robin, P. Day, *Adv. Inorg. Radiochem.* 1968, **10**, 247.

8 H. Wolfram, Dissertation 1900, Königberg.

9 (a) M. Tanaka, S. Kurita, T. Kojima, Y. Yamada, *Chem. Phys.* 1984, **91**, 257; (b) Y. Wada, T. Mitani, M. Yamashita, T. Koda, *J. Phys. Soc. Jpn.* 1985, **54**, 3143.

10 (a) R. J. H. Clark, M. L. Franks, W. R. Trumble, *Chem. Phys. Lett.* 1976, **41**, 287; (b) R. J. H. Clark, M. Kurmoo, D. N. Mountney, H. Toftlund, *J. Chem. Soc., Dalton Trans.* 1982, **9**, 1851; (c) R. J. H. Clark, *Chem. Soc. Rev.* 1990, **19**, 107.

11 H. Tanino, K. Kobayashi, *J. Phys. Soc. Jpn.* 1983, **52**, 1446.

12 K. Toriumi, Y. Wada, T. Mitani, S. Bandow, M. Yamashita, Y. Fujii, *J. Am. Chem. Soc.* 1989, **111**, 2341.
13 H. Kishida, H. Matsuzaki, H. Okamoto, T. Manabe, M. Yamashita, Y. Taguchi, Y. Tokura, *Nature* 2000, **405**, 929.
14 (a) S. Iwai, M. Ono, A. Maeda, H. Matsuzaki, H. Kishida, H. Okamoto, Y. Tokura, *Phys. Rev. Lett.*, 2003, **91**, 057401.
15 (a) S. Takaishi, Y. Tobu, H. Kitagawa, A. Goto, T. Shimizu, T. Okubo, T. Mitani, R. Ikeda, *J. Am. Chem. Soc.*, 2004, **126**, 1614; (b) S. Takaishi, M. Yamashita, H. Matsuzaki, H. Okamoto, H. Tanaka, S. Kuroda, A. Goto, T. Shimizu, T. Takenobu, Y. Iwasa, *Chem. Eur. J.*, 2008, **14**, 472.
16 (a) H. Matsuzaki, H. Okamoto, *in Material Designs and New Physical Properties in MX- and MMX-Chain Compounds*, ed. M. Yamashita and H. Okamoto, Springer, Wien, 2013, ch. 5, pp. 55–82; (b) H. Kishida, H. Okamoto, *ibid.*, ch. 7, pp. 93–109.
17 H. Okamoto, Y. Shimada, Y. Oka, A. Chainani, T. Takahashi, H. Kitagawa, T. Mitani, K. Toriumi, K. Inoue, T. Manabe, M. Yamashita, *Phys. Rev. B*, 1996, **54**, 8438.
18 (a) H. Okamoto, T. Mitani, K. Toriumi, M. Yamashita, *M. Mater. Sci. Eng., B*, 1992, **13**, L9; (b) H. Okamoto, T. Mitani, *Prog. Theor. Phys., Suppl.*, 1993, **113**, 191.
19 (a) M. Yamashita, S. Takaishi, *Chem. Commun.*, 2010, **46**, 4438; (b) S. Takaishi, H. Wu, J. Xie, T. Kajiwara, B. K. Breedlove, H. Miyasaka, M. Yamashita, *Inorg. Chem.* 2010, **49**, 3694.
20 H. Okamoto, K. Toriumi, K. Okaniwa, T. Mitani, M. Yamashita, *Synth. Met.* 1991, **42**, 2791.
21 S. Takaishi, M. Takamura, T. Kajiwara, H. Miyasaka, M. Yamashita, M. Iwata, H. Matsuzaki, H. Okamoto, H. Tanaka, S. Kuroda, H. Nishikawa, H. Oshio, K. Kato, M. Takata, *J. Am. Chem. Soc.*, 2008, **130**, 12080.
22 S. Kumagai, S. Takaishi, B. K. Breedlove, H. Okamoto, H. Tanaka, S. Kuroda, M. Yamashita, *Chem. Commun.* 2014, **50**, 8382.
23 H. Matsuzaki, S. Takaishi, M. Takamura, S. Kumagai, M. Yamashita, H. Okamoto, *J. Phys. Soc. Jpn.* 2012, **81**, 074705.
24 H. Matsuzaki, M. Iwata, T. Miyamoto, T. Terashige, K. Iwano, S. Takaishi, M. Takamura, S. Kumagai, M. Yamashita, R. Takahashi, Y. Wakabayashi, H. Okamoto, *Phys. Rev. Lett.* 2014, **113**, 096403.
25 D. M. Roessler, *Brit. J. Appl. Phys.* 1965, **16**, 1119.
26 S. Tao, T. Miyagoe, A. Maeda, H. Matsuzaki, H. Ohtsu, M. Hasegawa, S. Takaishi, M. Yamashita, H. Okamoto, *Adv. Mater.*, 2007, **19**, 2707.
27 N. Kimizuka, S. H. Lee, T. Kunitake, *Inorg. Chem.*, 2000, **39**, 389.
28 K. Okaniwa, H. Okamoto, T. Mitani, K. Toriumi, M. Yamashita, M. *J. Phys. Soc. Jpn.*, 1991, **60**, 997.
29 H. Matsuzaki, M. Yamashita, H. Okamoto, *J. Phys. Soc. Jpn.* 2006, **75**, 123701.

This paper reviews the recent progress in one-dimensional charge-bistable Pd(III)/Pd(II,IV) coordination polymers, called MX chains. The phase transitions between Pd(II)–Pd(IV) mixed valence and Pd(III) averaged valence states induced by temperature, pressure and light have been demonstrated, suggesting that MX chains are good candidates for the material for optical switching devices.